JOURNAL OF MATERIALS SCIENCE LETTERS 13 (1994) 457–461

Microstructure of Ti–TiB_2 surface layers produced by laser particle injection

J. H. ABBOUD, D. R. F. WEST
Department of Materials, Imperial College of Science, Technology, and Medicine, London SW7 2BP, UK

Surface treatments of materials using high power CO_2 lasers typically involve moving a substrate under the laser beam and generating a melt zone; concurrently, metal or ceramic or a combination of metal + ceramic in the form of powder is introduced into the melted zone by a feeding device, or by preplacing the powder on the substrate surface before laser melting. The melted zone is cooled rapidly by heat conduction through the substrate. The method can be used to enhance wear, corrosion, and erosion resistance. For example, laser melting a CP Ti substrate with continuous feeding of aluminium has been used to generate surface layers of titanium aluminide which are potentially useful for improving the oxidation resistance [1, 2]. The layer dimensions and compositions can be controlled by appropriate selection of laser processing parameters (such as laser power, powder feed rate, traverse speed) [3]. The cooling rate is estimated to be typically $\sim 10^3\ K\,s^{-1}$ and the microstructures are characteristic of rapid solidification and rapid solid state cooling [4]. Rapidly solidified Ti–Si alloyed layers with silicon contents ranging between 6 and 20 at % were also produced by the addition of silicon into the laser melted zone of CP Ti substrate using different feeding rates [5]. The hardness increased from 200 for the CP Ti to $\sim 600 H_v$ for the Ti–20 at % Si alloy.

The addition of ceramic such as TiC or SiC in particulate form into the laser melted zone has been reported [6–8]. The laser parameters were controlled to achieve partial dissolution of the ceramic particles. Ayers *et al.* [8] have found that the injection to TiC into Ti–6Al–4V alloy led to a reduction in the coefficient of friction from 0.4 to 0.18. A recent report by the authors found that the injection of SiC into CP Ti leads to the formation of TiC and Ti_5Si_3 in an α' matrix with an increase in the hardness from 200 to $\sim 600\ H_v$ and a decrease in the erosion rate of 25% [9, 10]. The use of lasers to produce composites in the form of surface layers of thickness between 0.5 and 1 mm or as pellets of ~3 mm diameter has been explored recently [11, 12] Systems studied were Ti/SiC, Ti/TiB_2, Ti/B_4C, and Ti/BN. Enrichment of the matrix with the products of dissolution occurred (e.g. Si, C, B) leading to the formation of compounds such as TiC and TiB.

The present paper reports in detail the microstructure of CP Ti and a βTi alloy (Ti–15V–3Al–3Cr–3Sn) alloy after injection with TiB_2.

A CW CO_2 laser operated at 1.8 and 3 mm beam diameter was used for laser surface melting CP Ti of 1 mm thickness and βTi alloy of 2 mm thickness. TiB_2 powder of particle size between 50 and 75 μm was introduced into the laser melted zone using a feeding device. The process was carried out under shrouding using argon gas to minimize the contamination of the melt pool. The relative speed between the substrate and the laser beam was kept constant at $7\ mm\,s^{-1}$ and the feed rate of TiB_2 was $0.1\ g\,s^{-1}$. After laser melting samples were cut transversely through the injected zone and standard methods were used for metallography. Scanning electron microscopy (SEM) linked with energy dispersive spectrometry (EDS) was used for structural and compositional analysis. Thin foils were prepared for transmission (TEM) and scanning transmission electron microscopy (STEM) by cutting a slice 1 mm thick, parallel to the surface of the laser injected zone; each slice was ground down to approximately 300 μm thickness. Discs of 3 mm diameter were cut by spark erosion and were dimpled from both sides until a thickness of ~50 μm was obtained. Ion beam thinning was used to obtain electron transparent areas. X ray diffractometry (XRD) was carried out using CuK_α radiation. Microhardness measurements across the injected area were made (500 g load).

Fig. 1a shows a transverse section of CP Ti injected with TiB_2. The injected area had a conduction limited shape of width ~2 mm and thickness ~0.8 mm, and extended into the substrate to a depth of 0.5 mm. The distribution of the TiB_2 was nearly uniform. SEM showed that the TiB_2 was partially dissolved and a faceted phase nucleated at the TiB_2/matrix interface and within the matrix (Fig. 1b). EDS analysis showed that the composition of the phase is very close to TiB. TEM examination showed clearly the interface between the undissolved TiB_2 and TiB. The latter phase appeared as small equiaxed grains with faulted substructure (Fig. 1c) and as long plates/laths (Fig. 1d). SADP confirmed the crystal structure to be consistent with TiB. The region away from the undissolved TiB_2 showed plate/lath type crystals of TiB (Fig. 1e) and eutectic consisting of α' + TiB; the α' has a cph crystal structure and a high density of dislocations while the TiB crystals were narrow and shorter than the primary TiB crystals (Fig. 1f).

The injection of TiB_2 into the laser melted zone of βTi(15V–3Al–3Cr–3Sn) alloy, using the same process parameters as for the CP Ti, produced a similar microstructure (Fig. 2a, b and c). The microstructure of the matrix consisted of primary faceted TiB and eutectic of β + TiB. SEM/EDS and STEM

0261-8028 © *1994 Chapman & Hall*

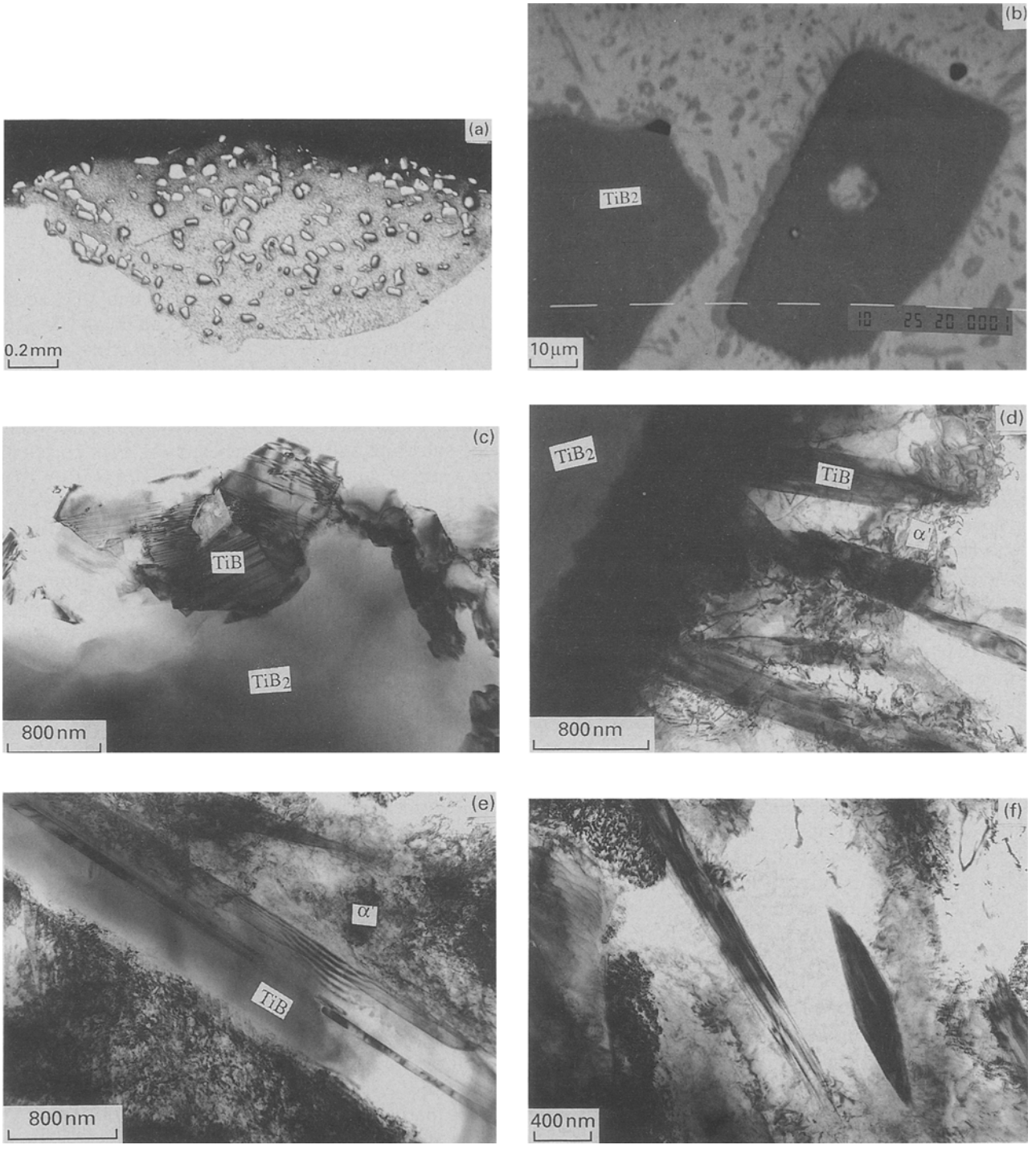

Figure 1 CP Ti injected with TiB_2, 1.8 kW laser power, 7 mm s^{-1} speed, 0.1 g s^{-1} powder flow rate: (a) optical macrograph showing a transverse section; (b) BSI-SEM micrograph showing TiB around TiB_2 and within the matrix: (c–f) TEM micrographs showing (c) equiaxed TiB region around TiB_2; (d) plate/lath TiB nucleated from the TiB_2; (e) primary TiB plate in α' matrix; and (f) eutectic TiB + α'.

analysis showed that the TiB contained 10 wt % V with traces of Al, Cr, and Sn (Table I). SADP confirmed the presence of some ω phase formed from β during rapid cooling. The average composition of the matrix (incorporating primary (Ti,V)B and eutectic but excluding the reaction rim) is shown in Table I. X-ray diffraction showed that the (Ti,V)B had 'd' values slightly smaller than those reported in the literature for TiB [13], consistent with the smaller atomic diameter of V. The average microhardness of the matrix was ~500 H_v as compared with the hardness of ~300 H_v of the substrate.

The Ti–B system shows TiB_2 as a compound congruently melting at 3225 °C with a range of stoichiometry of 1 wt % B. A peritectic reaction $L + TiB \rightarrow Ti_3B_4$ occurs at ~2200 °C, with another peritectic $L + Ti_3B_4 \rightarrow TiB$ at approximately 50 °C below the first reaction. TiB has a range of stoichiometry of 1 wt % B and is a constituent of the eutectic reaction L (2 wt % B) → B-Ti + TiB which occurs at ~1540 °C.

The maximum laser melt pool temperature is not known, but is likely to be in excess of the peritectic temperatures. There is extensive solubility of B in

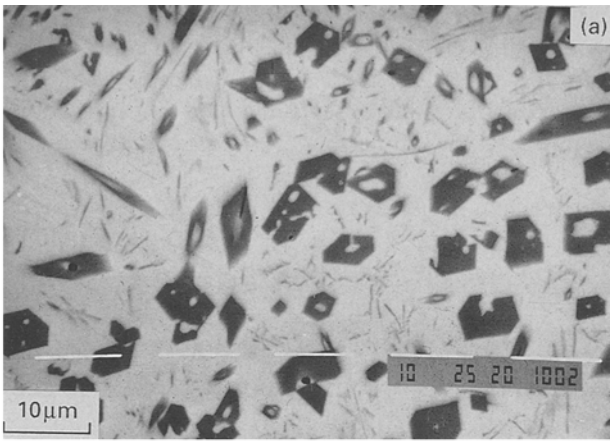

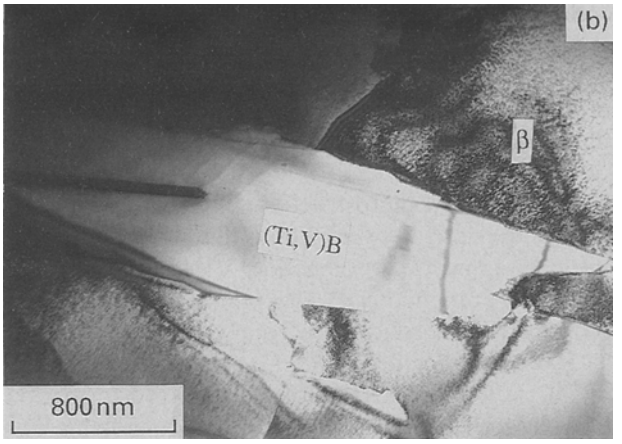

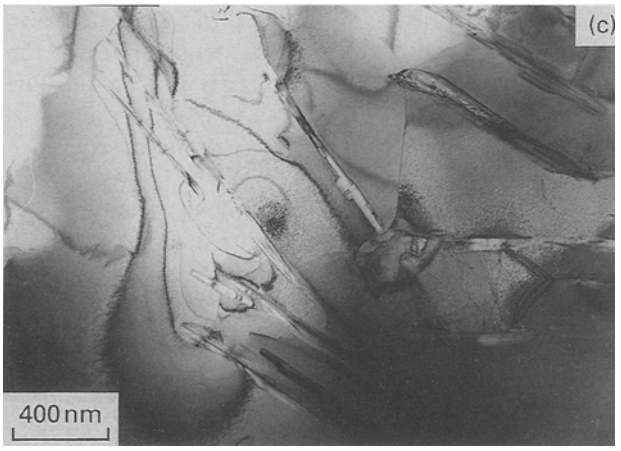

Figure 2 βTi (15V–3Al–3Cr–3Sn) alloy injected with TiB_2, 1.8 kW, 7 mm s^{-1}, 0.1 g s^{-1}: (a) SEM-BSI micrograph showing primary (Ti,V)B and eutectic of (Ti,V)B + β; (b and c) TEM micrographs showing primary (Ti,V)B in β phase (b) and eutectic structure β + (Ti,V)B (c).

TABLE 1 Compositional analysis data EDS/SEM (wt %)

Analysis	Ti	V	Al	Cr	Sn	B*
(Ti,V)B	72.5	10	0.1	0.1	0.2	~17
Matrix	74	13	2.6	2.3	2.8	~5.3

*Boron was calculated 'by difference'

liquid Ti as such temperatures; for example, at 2500 °C the phase diagram shows a solubility of ~16 wt % B. The short interaction times associated with the laser processing, i.e. of the order of 0.5 s, lead to incomplete solution of the TiB_2 particles, and a composition gradient will exist in the liquid adjacent to the particles. At the liquid/TiB_2 interface, assuming local equilibrium, the B content of the liquid will be the equilibrium solubility at the temperature considered. The average 'bulk' composition of the liquid will increase in B content with time at temperature as solution of TiB_2 in the liquid proceeds. During cooling and solidification from the maximum temperature down to the peritectic the B content of the liquid will decrease as some formation of TiB_2 occurs in the high B content liquid adjacent to the undissolved TiB_2. With the rapid cooling rate, neither of the peritectic reactions are expected to proceed to completion. On continued cooling below 2200 °C, primary plate-like crystals of TiB form, followed by the formation of the $\beta \rightarrow$ Ti + TiB eutectic (Fig. 1).

An approximate mass balance for the particle injection process can be carried out using the dimensions of the processed zone, and the proportions of the microstructural constituents, in relation to the phase diagram. The area of the build-up above the substrate surface for the situation shown in Fig. 1a is ~0.8 mm^2, representing approximately 30% of the area of the whole processed zone. This build-up area corresponds approximately to $fF/v\rho$, where f is the fraction of TiB_2 injected into the melt pool, F is the powder feed rate (mass/time), v is the traverse speed and ρ is the density of the feed powder [14]. Application of this relationship to the build-up area of Fig. 1a shows that f is only about 0.25, implying that powder loss during the processing is substantial; similar loss has been previously found [14] for alloying aluminium powder into titanium. Since the densities of TiB_2 and Ti are similar, the build-up area corresponds approximately to the weight % of TiB_2 injected into the melt pool, i.e. ~ 30 wt %. Assuming a mixture of completely undissolved TiB_2 and liquid titanium, a lever rule calculation gives an average composition of the composite melt pool of ~9 wt % B. The processed zone (Fig. 1a) contains ~15 vol (~15 wt %) of undissolved TiB_2. The matrix of the

zone consists of ~15 wt% primary TiB, with the remainder being the eutectic mixture; a lever rule calculation indicates an average B content of the matrix of 5 wt%. Applying a mass balance involving the undissolved TiB_2 and the matrix confirms a B content close to 9 wt%.

The electron microstructural observations of the interaction zone between liquid titanium and TiB_2 in the present work are generally consistent with the results of Prangnell *et al.* [15] on Ti–TiB_2 composite produced by a solid state route. No formation of Ti_3B_4 was detected and the reaction layer consisted of TiB; it was proposed [15] that the transformation of TiB_2 to TiB occurs at the interface moving into the TiB_2 particles, and that the B rejected is transported through the TiB layer into the titanium matrix. The TiB showed a substructure consisting of faulted regions similar to that observed in the present work (Fig. 1c). Also, needle-shaped faceted crystals of TiB developed, and it was proposed [15] that the growth maintained the flux of B atoms outwards for the reaction to proceed when matrix supersaturation with B is reached. In the present work, faulted plate/lath-like crystals extended outwards from the TiB layer, but in view of the high solubility for B in the liquid their formation is unlikely to be necessary for saturation reasons; they can be interpreted as primary crystals forming as the temperature decreases, similar to those formed in the bulk matrix.

In the case of the composite based on the βTi alloy, produced by laser melting a powder mixture of Ti and ceramic, similar microstructural features were observed, i.e. TiB formation around the TiB_2 particles, primary crystals of TiB and eutectic containing TiB. In contrast to the CP Ti-based composite, β phase was retained at room temperature instead of martensite formation occurring. The constitutional aspects may be interpreted by reference to a semi-schematic representation of the Ti–V–B phase diagram (Fig. 3). Neglecting the presence of the Al, Sn and Cr in the 15–3–3–3 alloy, the alloy composition is represented as containing 15 wt% on the Ti–V side of the compositional triangle. Assuming no preferential loss of alloying elements during processing the average composition of the composite zone lies on the line joining Ti–15 wt% V to TiB_2, and is shown (○) at ~38 wt% TiB_2 deduced from the dimensions of the build-up area. Partial solution of the TiB_2 leads to enrichment of the liquid in B, as in the case of the CPTi-based composite. From mass balance considerations, the average composition of the matrix lies on the line joining Ti–15V to (Ti,V)B, and, as shown in Fig. 3 the point designated ● representing matrix composition (Table I) agrees reasonably with this expectation. Application of the lever role to this line shows that the proportion of the undissolved TiB_2 should be around 20%, which agrees with the microscopical observations. From the estimated position of the $L \rightarrow \beta Ti + (Ti,V)B$ eutectic valley, the lever rule indicates that the proportion of primary (Ti,V)B should be ~20% which is also in reasonable agreement with the observed microstructure (Fig. 2a).

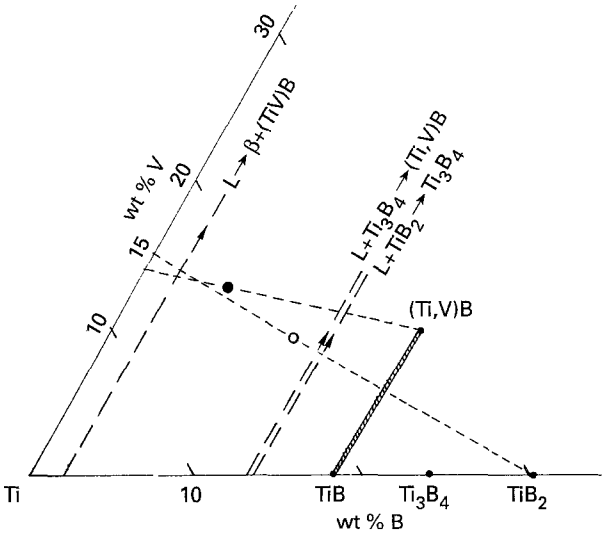

Figure 3 Ti–V–B system semi-schematic representation of phase relationships relevant to laser particle injection of βTi alloy with TiB_2, neglecting Al, Cr, and Sn. ○ = average composition of composite layer; ● = composition of matrix of composite (Table I) consisting of (Ti,V)B (containing ~10 wt% V) + βTi. – – – – estimated liquidus reaction curves, assumed to be approximately linear in relevant composition range (a possibility: not shown in Fig. 3, is that the $L + TiB_2 \rightarrow Ti_3B_4$ and $L + Ti_3B_4 \rightarrow$ (Ti,V)B curves may merge to give rise to a peritectic $L + Ti_3B_4 \rightarrow \beta Ti + (Ti,V)B$ and hence eutectic curve $L \rightarrow \beta Ti + (Ti,V)B$).

Acknowledgements

Acknowledgements are made to the Science and Engineering Research Council for financial support and to IMI Titanium Ltd, and TIMET for the provision of materials.

References

1. J. H. ABBOUD and D. R. F. WEST, *J. Mater. Sci. Lett.* **11** (1992) 1479.
2. A. HIROSE, T. UEDA and K. F. KOBAYASHI, *Mater. Sci. Eng.* **A160** (1993) 143.
3. J. H. ABBOUD and D. R. F. WEST, *Mat. Sci. Technol.* **7** (1991) 353.
4. *Idem. ibid.* **7** (1991) 827.
5. *Idem. Surf. Eng.* **7** (1991) 159.
6. J. D. AYERS and R. N. BOLSTER, in Proceedings of the Conference on Lasers in Metallurgy, February, 1981, edited by K. Mukherjee and J. Mazumdar (TMS-AIME, Warrendale, Pennsylvania, 1981) p. 115.
7. J. H. ABBOUD and D.R. F. WEST, *Mat. Sci. Technol.* **5** (1989) 725.
8. J. D. AYERS, T. R. TUCKER and R. C. BOWERS, *Scripta Metall.* **14** (1980) 549.
9. J. H. ABBOUD and D. R. F. WEST, *J. Mater. Sci. Lett.* **10** (1991) 1149.
10. J. J. ABBOUD, D. R. F. WEST and R. H. HIBBERD, *Surf. Eng.* **9** (3) (1993) 221.
11. *Idem.* Seventh World Conference on Titanium, San Diego, California, June 28–July 2, 1992.
12. *Idem. Mat. Sci. Technol.* to be published 1993.
13. N. B. PEARSON, "A handbook of lattice spacings and structures of metals and alloys", Vol. 1 (Pergamon, Oxford, 1958) p. 223.
14. R. REED, J. H. ABBOUD and D. R. F. WEST, in

Proceedings of International Conference on Laser Advanced Materials Processing Science and Applications, HIVE Nagaoka, Nagaoka, Niigata, Japan, 7–12 June, 1992, edited by A. Matsunawa and S. Katayama,
15. P. B. PRANGNELL, A. J. REEVES, T. W. CLYNE and W. STOBBS, in Proceedings of 2nd European Conference on Advanced Materials Processes, 22–24 July 1991, Vol. 2 edited by T. W. Clyne and P. J. Withers (The Institute of Materials, University of Cambridge, UK, 1992) p. 215.

Received 23 April
and accepted 16 August 1993